Preprint Title	Electromigration-induced directional steps towards formation of single atomic Ag contacts.
Authors	Atasi Chatterjee, Christoph Tegenkamp and Herbert Pfnür
Publication Date	28 Nov 2019
Article Type	Full Research Paper
ORCID® iDs	Christoph Tegenkamp - https://orcid.org/0000-0003-0453-0765; Herbert Pfnür - https://orcid.org/0000-0003-1568-4209

Electromigration-induced directional steps towards formation of single atomic Ag contacts.

A. Chatterjee[1,2], C. Tegenkamp[1,2,3] and H. Pfnür*[1,2]

Address: [1]Institut für Festkörperphysik, Leibniz Universität Hannover, Appelstraße 2, 30167 Hannover, Germany; [2]Laboratorium für Nano und Quantenengineering (LNQE), Leibniz Universität Hannover, Schneiderberg 39, 30167 Hannover, Germany and [3]Institut für Physik, Technische Universität Chemnitz, Reichenhainer Str. 70, 09126 Chemnitz

Email: H. Pfnür - pfnuer@fkp.uni-hannover.de

* Corresponding author

Abstract

Background: The process of electromigration is still not quantitatively understood. We showed recently that it can be used reliably for formation of single atomic point contacts in pre-structured Ag nanostructures.

Results: The process of formation of nanocontacts by electromigration (EM) down to a single atomic point contact was investigated for ultrathin (5 nm) Ag structures at 100 K. In this paper, we compare the structures with constrictions below the average grain size of Ag layers (15 nm), where the contribution of a single grain dominates, with structures of much larger constrictions of around 150 nm with multiple grains at the centre constriction during the initial steps of EM. The latter initially form filamentous structures. Despite these clear morphological differences, the conductance traces of both types of structures suggest that finally, i.e., in the quantized conduction regime, only one atomic point contact was formed. To analyse the thinning process within the semi-classical regime in detail, we used experimental conductance histograms in the range between $2\,G_0$ and $15\,G_0$ and their corresponding Fourier transforms (FT). The FT analysis of the conductance histograms exhibits a clear preference for thinning along the [100] direction. Using well-established

models, both atom-by-atom steps and ranges of stability, presumably caused by electronic shell effects, can be discriminated. A large range (5 to 14 G_0) of unstable conductance values was found in these electromigrated contacts that has not been reported by other techniques. It was observed irrespective of the initial geometry.

Conclusion: Although the directional motion of atoms during EM leads to specific properties like the instabilities mentioned, similarities to mechanically opened contacts with respect to cross sectional stability were found.

Keywords

electromigration; nanostructures; silver; Si substrate; focussed ion beam

Introduction

The transition from a three-dimensional (3D) conductor to single atomic chains is an intriguing process that has been addressed many times over the years. Its many aspects ranging from bulk solid state physics to the stability of various types of clusters, and their attachment to the environment to one-dimensional (1D) properties of atomic chains and contacts has been treated in many different studies [1-4]. However, the attraction to this topic is not only of pure scientific interest, it is also relevant in context with the reliable formation of ultra-small interconnects or of contacts of atomic size[5]. This latter topic is particularly challenging, since the exact value of the quantized contact resistance depends explicitly not only on the materials used and their valency [5,6], but also on the shape of the contact [5]. This is the reason why most studies only present histograms of the distribution of measured conductance values, since the exact local geometry at the contacts cannot be controlled.

Properties of metallic contacts of atomic size have been experimentally studied by using mechanically controllable break junctions (MCBJ), scanning tunneling microscopy (STM), electromigration (EM) and other techniques. All these techniques rely on conductance histograms as a statistical tool in order to find the configurations of high stability. Conductance histograms provide information about the most probable conductance values and their distribution around these values

that occur during the thinning process. Typically an overall probability distribution of several different measurements is taken that averages out possible instabilities and variations of the individual measurements. Both from experiments and theoretical simulations, partly going far beyond the free-electron model, give clear evidence for the existence of quantized conductance in atomic point contacts. The exact conductance values, however, turn out to depend significantly on the local contact configurations so that they may deviate from integer multiples of $2e^2/h$.[5,7]

Furthermore, conductance histograms of alkali metals and the direct comparison of conductance peak values with the magic numbers of cluster size suggest that the preferred electronic quantum modes influence the mechanically stable diameters [8,9]. This electronic shell effect was not only observed for alkali metals, but also in monovalent noble metals such as Ag and Au [10,11]. These experimental findings could be very well correlated with the theoretical simulations of conductance histograms [7,12,13]. The theoretical calculation of conductance histograms were based on the semi-classical interpretation of conductance quantisation proposed by Sharvin, where conductance is essentially proportional to the contact area [5,14]. The understanding of the origin of conductance histogram peaks can be deepened by searching for correlations between conductance values in the histograms. This information is contained in the Fourier transform (FT) of the conductance histograms. It also contains information about the structural thinning process, as demonstrated previously for several metallic systems [15-18], since, depending on the metal (fcc or bcc structure), the calculated ratios of frequencies in the FT were compatible with preferential growth in certain crystallographic high-symmetry directions.

Also our study uses these tools for data analysis. However, contrary to most EM experiments with thin metallic films on insulating substrates, the Ag/Si(100) system is unique in the sense that the first Ag layer wets the hydrogen terminated Si(100) surface [19], which improves the thermal contact so that thermally assisted processes during EM can be suppressed to a large extent, in agreement with own simulations [20]. For our experiments we use ultrathin Ag films (thickness 5 nm), which exhibit Stranski-Krastanov growth behavior so that they are nanocrystalline with an average grain size between 30 and 50 nm. These grain boundaries turned out to be the main source of lat-

eral resistance [21]. Therefore, the EM-induced material transport is mainly expected to take place at these boundaries. Furthermore, we were recently able to demonstrate very different behavior upon EM of such films depending on the size of the smallest constrictions. For bow-tie structures with a smallest constriction of typically 150 nm, generated by standard e-beam lithography, we observed EM-induced filamentuous structure formation at a surface temperature of 100 K. Visually a single electrically conducting path could not be identified nor reproducibly generated. This contrasts with experiments where the smallest constriction was reduced to one order of magnitude down to about 15 nm using a focused ion beam (FIB), i.e. far below the average grain size in the Ag film [22]. Under these conditions we obtained highly reproducible single atomic point contacts (more than 90% of the structures) with a well defined value of 1.3 G_0.

We thus have a very well defined reference system, generated by EM. Therefore, it seems to be meaningful to analyse more details about the thinning process induced by EM of this system from the information contained within the experimental conduction histograms and their FTs. Furthermore, since the morphological appearance of the EM-induced structuring process for the large structures appear to be fundamentally different, such a study could also clarifiy whether these differences also appear in the conduction histograms and their FTs.

Results and Discussion

In order to illustrate the importance of ultra-narrow structuring for getting reliable results, we present SEM images of Ag nano-structures before and after EM for bow-tie structures with centre width between 100 and 200 nm in comparison with FIB patterned bow-tie structures with centre widths $<$ 20 nm (see Fig. 1). EM in the wide Ag contact results in clear unidirectional material transport, as seen by the large clusters preferentially formed on the right side of Fig. 1b), appearing as white spots. However, a filamentous structure is always formed on the left side that neither allows to identify the exact location of the point contact nor allows reproducible production of point contacts. Nevertheless, quantized conductance plateaus as a function of time was still observed for these bow-tie structures during EM.

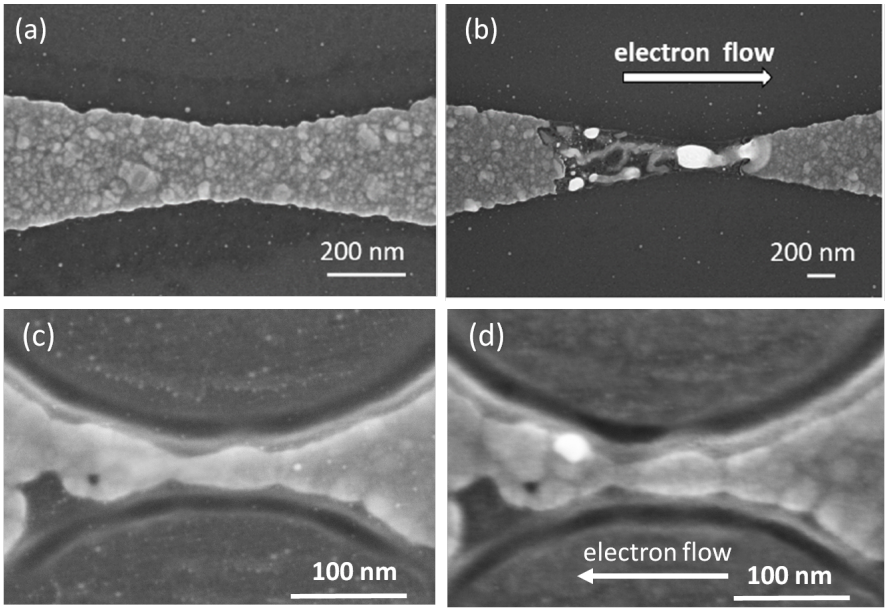

Figure 1: (a) Typical SEM image of a 5 nm thick, nano-crystalline Ag bow-tie structure before EM. (b) after EM yielding a conductance value around 1 G_0. (c) SEM of a further FIB-patterned bow-tie structure before EM with elliptical grooves reducing the centre constriction to 17 nm. Please note the different scale bar. (d) after EM yielding a conductance value of 1.3 G_0. (c) and (d) reproduced from ref. [22] with permission from AIP Publishing.

It turned out that the existence of several grains in the cross section of these Ag wires is the reason for this morphological behaviour. Since EM mainly occurs at the grain boundaries, the contact resistance between various grains has a comparable value due to similar sizes of grains and contact areas. Thus a complicated parallel EM process sets in, in this type of structure involving many grains. Material exchange between many of them leads to this filament-like growth of wires with, as far as we can judge, larger grains than before EM. However, since EM is a process with partial positive feedback, also thinning takes place, but the location cannot be well defined. Nevertheless, after a competition of several grains in the narrowest constriction, point contact is located in one of these filaments which is hard to locate structurally. Electrically these structures exhibit well defined conductance quantisation.

For a much better controlled process it turned out [22] that it is sufficient to reduce the number of grains at the centre to one. In this case, the current density is clearly highest at only one grain boundary so that the thinning process happens mainly there, as demonstrated by a comparison be-

tween Figs. 1c) and d). For these very narrow structures we obtained highly reproducible values of final conductance in about 95% of the structures investigated.

We now want to address the question how the thinning process in these morphologically quite different structures proceeds under conditions of EM and at temperatures, at which thermal diffusion is largely suppressed [20]. Due to the high probability of electron scattering at grain boundaries, material transport mainly happens at and across grain boundaries, but not within homogeneous crystalline material that is typically assumed in most models. Therefore, deviations from these models must be expected. Focussing for the moment on a single grain boundary, the directed material transport in EM will cause thinning of one grain while the other has to take up the material. Thus a strong asymmetry is introduced, which is absent in the case of mechanically controlled break junction experiments so that these two types of experiments may yield different results. Furthermore, we will show that the chosen starting conditions (bow-tie and FIB patterned bow-tie structures), which result in significantly different structure formation during the EM process, undergo similar steps of thinning and will finally end up both in single junctions. In order to avoid the pure quantum regime and to understand the mechanism during thinning, we concentrate only on the semi-classical region. Therefore all the conductance histograms discussed here starts at $2\,G_0$.

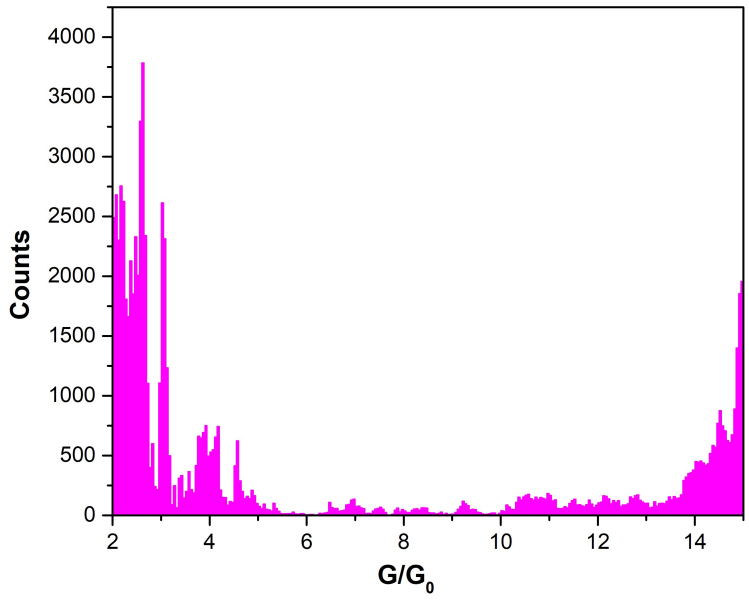

Figure 2: Conductance histogram of conductance traces of bow-tie electromigrated structures.

The conductance histogram obtained from the conductance traces during EM of bow-tie structures is depicted in Fig. 2. This histogram shows distinct peaks between $2\,G_0$ and $15\,G_0$. 20 conductance traces during EM thinning were averaged. In Fig. 2 peaks at $2.1\,G_0$, $2.6\,G_0$, $3.0\,G_0$, $3.8\,G_0$, $4.2\,G_0$, $4.6\,G_0$, $14.5\,G_0$ and $15\,G_0$ are observed. Non-integer values of conductance are commonly observed [18,23,24] mainly due to the asymmetric and slightly irregular shape of the contact. It was also found in theoretical simulations [7].

It is remarkable that between 4.5 and 14 G_0 there is a large range of instability, i.e. once the critical conductance falls short of $14\,G_0$, further EM barely finds stable configurations until values below $5\,G_0$ are reached. This large range of instability indicates either a break-up of several contacts ($G > 15G_0$) into a single contact or an instability of a single contact. The first scenario is not very probable. Since about 20 structures were used and averaged, which have various starting geometries and a different number of wires at large G, it is not plausible to expect an instability at the same overall G value. Therefore, we conclude that already at values around $15\,G_0$ it is essentially only one wire that is conducting. Such instabilities seem to be characteristic to the EM process, since they are commonly not observed in a MCBJ experiment, but have also been found in recent EM experiments in Cu nano-contacts [18]. Since a distribution of wires of various sizes exist, there is still a small probability for conductance through more than one channel that is reflected by the small number of counts in the range between 14 and $5\,G_0$.

On performing a FT of this conductance histogram (see Fig. 3), a distinct peak structure is observed that corresponds to characteristic decrements of conductance. It can be interpreted by the semi-classical Sharvin formula. This formula is an approximation for contacts approaching the ballistic regime. Within this model, the nano-wire conductance for a circular cross-sectional area A is given by [15]

$$g = \frac{G}{G_0} = \pi A - (\pi A)^{1/2} + 1/6 \tag{1}$$

$$G = gG_0 = G_0\left[\left(\frac{k_F R}{2}\right)^2 - \frac{k_F R}{2} + 1/6\right] \quad (2)$$

with the Fermi wavelength $\lambda_F = 2\pi/k_F$. In eq. 2 the cross-sectional area A is expressed in units of ${\lambda_F}^2$. Taking into account the spillout of electron density beyond the rectangular potential assumed in Sharvin's model, the two last terms in eqs. 1 and 2 nearly cancel [15]. This brings in a linear relationship between A and g ($\Delta g = \pi \Delta A$).

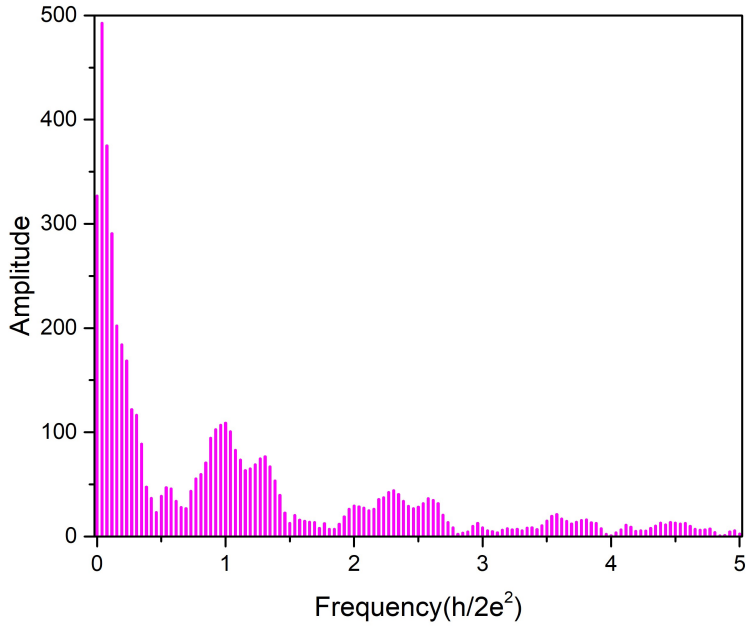

Figure 3: FT of conductance histogram of bow-tie electromigrated structures shown in Fig. 2.

If we ignore for the moment the different orientation of grains - for a justification, see below - and assume that only a single contact is thinned at a time, we can use a previously developed argumentation [15,25]: Considering fcc packing in the direction perpendicular to the three principal directions [111], [100], and [110], 2-dimensional contact areas and their conductance can be identified. The area of the 2D (111), (100), and (110) unit cells is $\sqrt{3}/2a^2$, a^2 and $\sqrt{2}a^2$ respectively. Here a is the lattice constant. If a one-by-one atom decrement of the contact areas of a crystalline grain is considered, the conductance steps have different sizes that scale with $\Delta g_{111} : \Delta g_{100} : \Delta g_{110} =$ 0.87:1:1.41 for thinning along these directions. Taking k_F of bulk Ag, the calculated periods in

the three principal directions correspond (in units of G_0) to Δg_{100}=0.96, Δg_{111}=0.83, Δg_{110}=1.36. The inverse conductance values should appear in the FT of a conductance histogram as $(\Delta k_F R)^{-1}$, where spacing between G values corresponds to a specific direction. The frequencies obtained from eqs. 1 and 2 for an fcc crystal structure are $0.8\,G_0^{-1}$,$1\,G_0^{-1}$ and $1.3\,G_0^{-1}$ for the three principal crystallographic directions [110],[100] and [111], respectively [15].

In order to apply this theory to the thinning at grain boundaries, we have to recall two facts: Firstly, in nanocrystalline elemental material like Ag grain boundaries occur mostly because of different orientation of nanocrystals. Since the elastic strain energy strongly increases with angular misfit, small angle grain boundaries are the most likely ones. Thus most contact areas are not far from (stepped) high symmetry crystal planes. Secondly, due to its high directionality, EM thins one grain while depositing the material on an adjacent grain. Therefore, the local electrical resistance is determined by the contact area of the grain that is thinned to the adjacent grain that is taking up the material. Only this cross section and its variation by EM is considered. Thus deviations due to unknown step densities and local strain are ignored when considering only high symmetry directions of the interface, as is done in the following.

Fig. 3 represents the FT of the conductance histogram in Fig. 2 of bow-tie structures between $2\,G_0$ and $15\,G_0$. The most dominant frequencies are $1\,G_0^{-1}$ and $1.3\,G_0^{-1}$. Other peak frequencies in Figure 3 are at $0.6\,G_0^{-1}$, $2.1\,G_0^{-1}$, $2.3\,G_0^{-1}$ and $2.6\,G_0^{-1}$. The large peaks below 0.2 h/2e^2 are characteristic of large jumps in the conductance histograms, as already pointed out in Figure 2, and again denote the instability of intermediate conductance values between 14 and $5\,G_0$.

The dominant frequencies at $1\,G_0^{-1}$ and $1.3\,G_0^{-1}$ in Fig. 3 agree within error bars quantitatively with those derived above for atom-by-atom thinning [15] in [100] and [111] directions during EM. Within this argumentation, it is also interesting to see that the contribution from $0.8\,G_0^{-1}$, i.e. thinning in [110] direction, is absent in these structures. This result contrasts with a MCBJ experiment in Au nano-wires [15], in which all three frequencies were obtained. It matches, however, with the findings of mechanical stretching experiments of Ag nanowires, observed with HRTEM [26], where it was reported that Ag mostly forms rod-like structures for [110] directions, which are un-

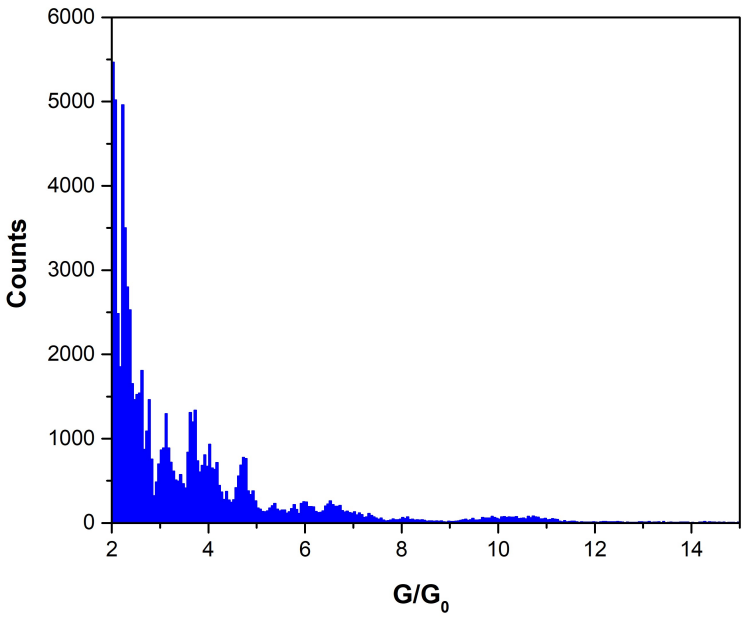

Figure 4: Conductance histogram of conductance traces obtained during EM of FIB patterned structures.

able to from wires. Atomic chains turned out to form only when at least one grain was oriented in [100] direction. The dominant peak at 1 G_0^{-1} in Fig. 3 indeed indicates thinning in this particular direction. From these dominant peaks in the FT and the HRTEM results [26], we conclude that the relevant structures in the conductance window considered here consist preferentially of single junctions that make contact either in [100] or [111] directions.

The frequency at 0.6 G_0^{-1} has also been observed before, by Mares et al. [10] which was attributed to relatively stable cross sections due to the formation of diametric orbits. This frequency was found to be very prominent for Ag, less prominent in Cu and absent in Au as observed by the authors of [10]. Along the same lines, the very interesting significance of the 1 G_0^{-1} peak is the superposition of square and triangular orbits [5,10].

The frequencies between 2 G_0^{-1} and 3 G_0^{-1} contain clearly the overtones of those frequencies just discussed with prominent peaks at 2 G_0^{-1} and 2.6 G_0^{-1}, but also a small peak at 2.3 G_0^{-1}, which does not fit into the simple picture just described. These are contributions from the spacings of metastable configurations with changes of conductance on the sub-G level due to local changes in the close environment of the actual contact. Such sub-G spacings between conductance values

can be clearly spotted from the conductance histogram in Fig. 2 and have also been observed in simulations of Ag nanocontacts [7].

The results of the FIB patterned bow-tie structures essentially corroborate the assumptions made above that essentially a single junction was measured already starting with mesoscopic bow-tie structures. The conductance histogram for the structures thinned with FIB to a single grain contact for the same range of G as in Fig. 2, using the average of 15 conductance traces, is shown in Fig. 4. A quite similar peak structure as in Fig. 2 is seen there between 2 G_0 and 5 G_0. There are strong peaks at 2.1 and 2.3 G_0 but less intense peaks at 2.6 G_0 as compared to Fig. 2, but in general, there is no large qualitative difference between the conductance histograms of Figs. 2 and 4 below 5 G_0. However, the peaks around 14.5 and 15 G_0 are absent in Fig. 4, i.e. the range of unstable cross sections is even more extended in this case. This difference may be due to the size distribution of grains in Fig. 2, which smears out the range of instability, whereas the results summarized in Fig. 4 were obtained from single grains as the starting configuration. In this situation, there is less possibility for particle exchange between different grains that may reduce the range of visible instabilities.

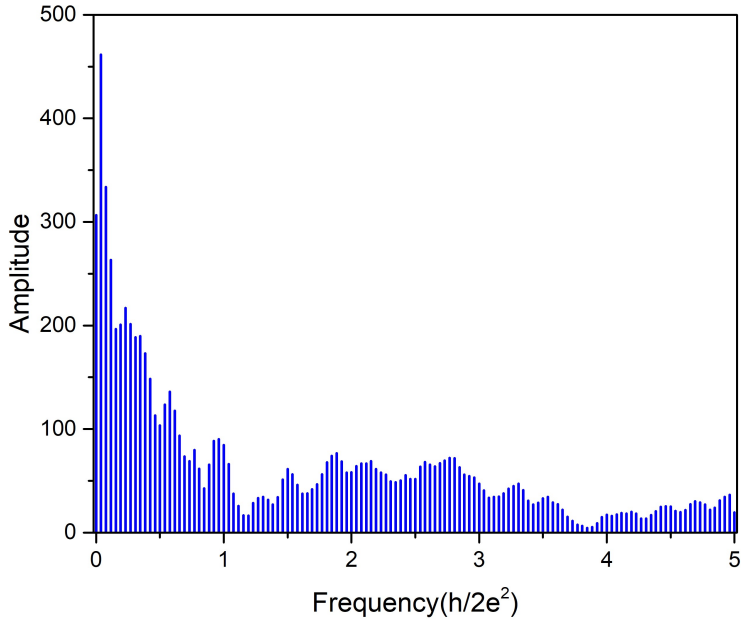

Figure 5: FT of conductance histogram of FIB patterned structures shown in Figure 4.

At first sight, the FT of Fig. 4, shown in Fig. 5, looks very similar to that shown in Fig. 3, again sup-

porting our hypothesis that also in the large bow-tie structures we observe only thinning of a single grain in the range of conductance below 15 G_0. As concluded from the peak position at 1 G_0^{-1}, preferential thinning at [100]-oriented grain boundaries occurs. Coming back to the electronic shell effects, this dominance of peak at 1 G_0^{-1} in both types of structures not only gives evidence that the atomic point contact thinning occurs at the [100] oriented interface, but also demonstrates the prominence of the electronic shell effect [10] in these ultra thin Ag films at 100 K.

A further similarity with Fig. 3 is the presence of the peak at 0.6 G_0^{-1}. Strong peaks below 0.5 G_0^{-1} again correspond to the instabilities between other metastable configurations.

On the other hand, the [111] orientation is missing: there is no peak above noise level at 1.3 G_0^{-1}. Since FIB structuring is not expected to be selective with respect to the grain orientation, this finding proves that only grains with material exchange along the [100] direction participate in the atomic point contact formation. Assuming that the [100] thinning direction is the energetically most likely one, the [111]-direction is only observed when the contribution from multiple grains cannot be completely ignored. Thus the [111] direction appears in Fig. 3, but with less probability than [100], whereas [110] was never seen.

Interestingly, the structure between 1.5 G_0^{-1} and 3 G_0^{-1} in Fig. 5 is somewhat more extended and more pronounced than in Fig. 3. While the reasons for its occurrence are similar to those mentioned in context with the latter figure, the histogram of Fig. 4 exhibits finer peak spacings in comparison to Fig. 2 that gives a different weight to the overtones between 1.5 and 3 G_0^{-1} in Fig. 5.

Conclusions

The EM process in ultrathin nanocrystalline Ag structures on Si(100) was investigated for structures that had a narrowest constriction of 100 to 150 nm. These were compared with those further structured by FIB down to 15 nm, i.e. below the individual grain size. Although the mesoscopic evolution of structures with filament formation for the large structures was very different from the initially only 15 nm wide structures, the similarity of conductance histograms below 15 G_0 lead us to the conclusion that only a single contact existed in most cases. A large range of unstable con-

figurations between 14 and 5 G_0 may be characteristic for the EM process at a temperature where only limited thermal diffusion is possible, since such a range of instability was not found in experiments with other techniques. At this point, due to the limited available data set involving only Ag contacts, it remains unclear how general this phenomenon is. However, it may be related to the observed instability of other thinning directions for Ag.

Although the thinning mechanism of EM seems to be quite different from that during mechanical stretching, we conclude form our FT analysis that the underlying atomistic processes seem to be quite comparable. Similar conclusions are drawn in ref. [27]. This similarity can be rationalized from the fact that although EM is directional and, therefore, generates asymmetric contacts, only the narrowest constriction plays the crucial role, so that the exact shape of the contact is comparatively unimportant. The detailed investigation, taking the FTs of conduction histograms, revealed a preference for atom-by-atom thinning along the [100] direction and a combination of geometric and electronic shell effects [15].

This study thus complements existing data from MCBJ measurements of Ag and HRTEM investigations on Ag point contacts and provides a concrete information on the mechanism of thinning in ultra-thin Ag films.

Experimental Details

Low-doped Si(100) substrates (1000Ω-cm at 300 K) were used that are good insulators at temperatures around 100 K. Structuring was done by a triple-step process: As a first step, we patterned the contact pads by photolithography. Secondly, electron beam lithography was employed in order to get nanostructures of bow-tie shape that were 100 to 200 nm wide at the smallest constriction. After HF dip, in order to get a hydrogen terminated surface, one monolayer of Ti served as wetting layer before we evaporated 5 nm of Ag onto it at room temperature. Thirdly, these bow-tie structures were further patterned by a FIB in order to reduce the centre width below the size of a single grain. By writing elliptical structures into the Ag nanostructures, we were able to reduce the centre

width of the nanostructures to below 20 nm. The detailed steps involved in the sample fabrication were reported in a previous publication [20,22].

All measurements were performed within a 4-tip SEM/STM UHV chamber (base pressure 2×10^{-10} mbar). This facilitated cooling of the structures down to 100 K without any spurious condensation on them. Furthermore, the UHV environment was important for the Ag structures as they were quite susceptible to sulphur contamination in ambient conditions. UHV also provided an ultra-clean environment for point contact measurements. Two out of the four available tips were used for the EM measurements. The tips were pre-cooled by making electrical (and mechanical) contact with the contact pads produced by photolithography.

To perform EM measurements, an in-house LabVIEW program was developed (following Motto et al. [28]), that allowed precise control of conductance in order to obtain atomic point contacts. Suitable feedback parameters and ramp speeds for the applied bias voltage were selected in the program which consisted of two feedback loops. The starting resistance of the structures were typically between 50-100 Ω. When the resistance change between two consecutive measurements was less than the preset value, the ramp voltage was increased. In the other case, the control went to the second loop, where momentary resistance changes (due to structural changes) were compared with preset feedback parameters with a response time of 10 ms. Abrupt changes in resistance took place at current densities of $5 \pm 2 \times 10^{13}$ A/m^2 and at voltages between 0.8 V and 1.5 V, depending on the actual structure.

Conductance traces were obtained during EM thinning, which demonstrated step-like conductance plateaus. Details of EM thinning can also be found in our earlier publication [22]. Conductance histograms constructed using these plateaus revealed the most probable (and temporally stable) conductance values as peaks. Finally a FT analysis of these experimental conductance histograms was performed to identify the crystallographic contributions of the metallic structure.

Acknowledgements

We acknowledge financial support by the Hannover School of Nanotechnology (HSN).

References

1. Agrait, N.; Rodrigo, J. G.; Vieira, S. *Phys. Rev. B* **1993**, *47* (18), 12345–12348. doi:10.1103/physrevb.47.12345.

2. Krans, J. M.; van Ruitenbeek, J. M.; Fisun, V. V.; Yanson, I. K.; de Jongh, L. J. *Nature* **1995**, *375* (6534), 767–769. doi:10.1038/375767a0.

3. van Ruitenbeek, J. M.; Alvarez, A.; Piñeyro, I.; Grahmann, C.; Joyez, P.; Devoret, M. H.; Esteve, D.; Urbina, C. *Review of Scientific Instruments* **1996**, *67* (1), 108–111. doi:10.1063/1.1146558.

4. Yanson, A. I.; Yanson, I. K.; van Ruitenbeek, J. M. *Physical Review Letters* **2000**, *84* (25), 5832–5835. doi:10.1103/physrevlett.84.5832.

5. Agraït, N.; Yeyati, A. L.; van Ruitenbeek, J. *Phys. Rep.* **2003**, *377* (2), 81 –279. doi:10.1016/S0370-1573(02)00633-6.

6. Smit, R. H. M.; Untiedt, C.; Yanson, A. I.; van Ruitenbeek, J. M. *Phys. Rev. Lett.* **2001**, *87* (26), 266102. doi:10.1103/physrevlett.87.266102.

7. Pauly, F.; Dreher, M.; Viljas, J. K.; Häfner, M.; Cuevas, J. C.; Nielaba, P. *Physical Review B* **2006**, *74* (23), 235106. doi:10.1103/physrevb.74.235106.

8. Yanson, A. I.; Yanson, I. K.; van Ruitenbeek, J. M. *Nature* **1999**, *400* (6740), 144–146. doi:10.1038/22074.

9. Yanson, A. I.; Yanson, I. K.; van Ruitenbeek, J. M. *Physical Review Letters* **2001**, *87* (21), 216805. doi:10.1103/physrevlett.87.216805.

10. Mares, A. I.; van Ruitenbeek, J. M. *Physical Review B* **2005**, *72* (20), 205402. doi:10.1103/physrevb.72.205402.

11. Obermair, C.; Kuhn, H.; Schimmel, T. *Beilstein Journal of Nanotechnology* **2011**, *2*, 740–745. doi:10.3762/bjnano.2.81.

12. Hasmy, A.; Medina, E.; Serena, P. A. *Physical Review Letters* **2001**, *86* (24), 5574–5577. doi: 10.1103/physrevlett.86.5574.

13. Dreher, M.; Pauly, F.; Heurich, J.; Cuevas, J. C.; Scheer, E.; Nielaba, P. *Physical Review B* **2005**, *72* (7), 075435. doi:10.1103/physrevb.72.075435.

14. *Mesoscopic Electron Transport*; Sohn, L. L., Kouwenhoven, L. P., Schön, G., Eds.; Springer Netherlands, 1997; doi:10.1007/978-94-015-8839-3.

15. Yanson, I. K.; Shklyarevskii, O. I.; Csonka, S.; van Kempen, H.; Speller, S.; Yanson, A. I.; van Ruitenbeek, J. M. *Physical Review Letters* **2005**, *95* (25), 256806. doi:10.1103/physrevlett.95.256806.

16. Yanson, I. K.; Shklyarevskii, O. I.; van Ruitenbeek, J. M.; Speller, S. *Physical Review B* **2008**, *77* (3), 033411. doi:10.1103/physrevb.77.033411.

17. Shklyarevskii, O. I.; Yanson, I. K. *Low Temperature Physics* **2013**, *39* (3), 285–288. doi:10.1063/1.4795200.

18. Pfender-Siedle, R.; Hauser, J.; Hoffmann-Vogel, R. *Phys. Rev. B* **2017**, *95* (23), 235418. doi: 10.1103/physrevb.95.235418.

19. Tanaka, Y.; Kinoshita, T.; Sumitomo, K.; Shoji, F.; Oura, K.; Katayama, I. *Appl. Surf. Sci.* **1992**, *60-61*, 195 –199. doi:10.1016/0169-4332(92)90416-U.

20. Chatterjee, A.; Bai, T.; Edler, F.; Tegenkamp, C.; Weide-Zaage, K.; Pfnür, H. *J.Phys.: Condensed Matter* **2018**, *30*, 084002. doi:10.1088/1361-648x/aaa80a.

21. Schmeidel, J.; Pfnür, H.; Tegenkamp, C. *Phys. Rev. B* **2009**, *80*, 115304. doi:10.1103/PhysRevB.80.115304.

22. Chatterjee, A.; Heidenblut, T.; Edler, F.; Olsen, E.; Stöckmann, J. P.; Tegenkamp, C.; Pfnür, H. *Applied Physics Letters* **2018**, *113* (1), 013106. doi:10.1063/1.5040405.

352 23. Li, C. Z.; Bogozi, A.; Huang, W.; Tao, N. J. *Nanotechnology* **1999**, *10* (2), 221–223. doi:10.
353 1088/0957-4484/10/2/320.

354 24. Bettini, J.; Rodrigues, V.; González, J.; Ugarte, D. *Appl. Phys. A* **2005**, *81* (8), 1513–1518.
355 doi:10.1007/s00339-005-3388-9.

356 25. Rodrigues, V.; Ugarte, D. *Nanotechnology* **2002**, *13* (3), 404–408. doi:10.1088/0957-4484/13/
357 3/332.

358 26. Rodrigues, V.; Bettini, J.; Rocha, A. R.; Rego, L. G. C.; Ugarte, D. *Phys. Rev. B* **2002**, *65* (15),
359 153402. doi:10.1103/physrevb.65.153402.

360 27. Klavsyuk, A. L.; Saletsky, A. M. *Uspekhi Fizicheskih Nauk* **2015**, *185* (10), 1009–1030. doi:
361 10.3367/ufnr.0185.201510a.1009.

362 28. Motto, P.; Dimonte, A.; Rattalino, I.; Demarchi, D.; Piccinini, G.; Civera, P. *Nanoscale Res.*
363 *Lett.* **2012**, *7* (1), 113. doi:10.1186/1556-276x-7-113.